Comparison of phosphorescent agents for noninvasive sensing of tumor oxygenation via Cherenkov-excited luminescence imaging

Jennifer R. Shell
Ethan P. LaRochelle
Petr Bruza
Jason R. Gunn
Lesley A. Jarvis
David J. Gladstone
Brian W. Pogue

SPIE.

Comparison of phosphorescent agents for noninvasive sensing of tumor oxygenation via Cherenkov-excited luminescence imaging

Jennifer R. Shell,[a,*,†] Ethan P. LaRochelle,[a,†] Petr Bruza,[a] Jason R. Gunn,[a] Lesley A. Jarvis,[b] David J. Gladstone,[a,b] and Brian W. Pogue[a]
[a]Dartmouth College, Thayer School of Engineering, Hanover, New Hampshire, United States
[b]Dartmouth College, Geisel School of Medicine, Hanover, New Hampshire, United States

Abstract. Cherenkov emission generated in tissue during radiotherapy can be harnessed for the imaging biochemistry of tissue microenvironments. Cherenkov-excited luminescence scanned imaging (CELSI) provides a way to optically and noninvasively map oxygen-related signals, which is known to correlate to outcomes in radiotherapy. Four candidate phosphorescent reagents PtG4, MM2, Ir(btb)$_2$(acac), and MitoID were studied for oxygen sensing, testing in a progressive series of (a) in solution, (b) *in vitro*, and (c) in subcutaneous tumors. In each test, the signal strength and response to oxygen were assessed by phosphorescence intensity and decay lifetime measurement. MM2 showed the most robust response to oxygen changes in solution, followed by PtG4, Ir(btb)$_2$(acac), and MitoID. However, in PANC-1 cells, their oxygen responses differed with Ir(btb)$_2$(acac) exhibiting the largest phosphorescent intensity change in response to changes in oxygenation, followed by PtG4, MM2, and MitoID. *In vivo*, it was only possible to utilize Ir(btb)$_2$(acac) and PtG4, with each being used at nanomole levels, to determine signal strength, lifetime, and pO$_2$. Oxygen sensing with CELSI during radiotherapy is feasible and can estimate values from 1 mm regions of tissue when used in the configuration of this study. PtG4 was the most amenable to *in vivo* sensing on the timescale of external beam LINAC x-rays. © *The Authors. Published by SPIE under a Creative Commons Attribution 4.0 Unported License. Distribution or reproduction of this work in whole or in part requires full attribution of the original publication, including its DOI.* [DOI: 10.1117/1.JBO.24.3.036001]

Keywords: tumor hypoxia; Cherenkov radiation; phosphorescence; optical imaging.

Paper 180604R received Oct. 31, 2018; accepted for publication Feb. 1, 2019; published online Mar. 4, 2019.

1 Introduction

Extent of oxygenation in tumors is a known indicator of the success of radiation therapy, partly due to the oxygen enhancement ratio,[1] as well as due to oxygen being a surrogate marker for other features of tumor aggressiveness.[2] Therefore, monitoring of tumor oxygenation during fractionated radiation therapy would be advantageous to gauge the likelihood of response or even to estimate if treatment plan alternations such as a boost to hypoxic areas might be beneficial. Oxygen electrodes have been utilized to measure hypoxia.[3–5] While this method allows direct measurement of oxygen levels in tumors, it is invasive and is limited to tumors that are easily accessible. Tumor biopsies with indirect measurements for hypoxia, including pimonidazole staining and immunostaining for HIF-1α, provide valuable information of individual tumor microenvironments,[6–10] but these methods are also invasive and do not provide real-time measurement of tumor oxygenation levels. Blood oxygen level-dependent magnetic resonance imaging (BOLD-MRI),[11,12] electron paramagnetic resonance oximetry,[13,14] and near-infrared spectroscopic tomography[15] provide real-time information based on hemoglobin saturation. Positron emission tomography also measures real-time levels of hypoxia, utilizing ^{18}F-labeled nitroimidazole derivatives, whose luminescence are dependent on oxygen levels.[16,17] Despite the potential value, there has not been any clinical convergence on a method for imaging tumor oxygenation that is noninvasive, precise, and quantitative. In this study, oxygen-related mapping in tumors is demonstrated with Cherenkov-excited luminescence scanned imaging (CELSI), which uses the inherent delivery of radiation to get maps of oxygen-dependent luminescence signals from injected chemical sensors. Current reagents utilized for phosphorescent sensing of oxygen that can be utilized for noninvasive determination of oxygen content [PtG4, MM2, Ir(btb)$_2$(acac), and MitoID] are evaluated.

Radiation treatment with MV photons or MeV electrons causes the production of Cherenkov light in tissue. This optical emission occurs when charged primary or secondary electrons pass through the dielectric medium, such as tissue, at a velocity greater than the speed of light. This optical signal has been imaged to visualize surface dose in radiation therapy.[18–20] In addition, early pilot studies in tissue phantoms and individual animals have shown utilization of Cherenkov emission as the excitation source in imaging applications, including the detection of fluorophores and phosphors in conjunction with radiation therapy.[21] The potential to sense tumor oxygenation through CELSI with the phosphorescent reagent PtG4 has been shown by us, because the PtG4 phosphorescence is quenched in the presence of oxygen, reducing the observed lifetime of emission. In the presence of ambient oxygen pressure (pO$_2$), the PtG4 phosphorescence lifetime is 16.9 μs, and in low pO$_2$ it is 47 μs.[22,23]

In this study, this agent was compared to other oxygen-quenched chemical agents, and each was examined for its potential to sense tumor hypoxia by directly measuring pO$_2$ levels *in vivo* with mice bearing subcutaneous tumors.[24] At the end of the

*Address all correspondence to Jennifer R. Shell, E-mail: jennifer.r.shell@dartmouth.edu

†Jennifer R. Shell and Ethan P. LaRochelle contributed equally to this work.

study, the spatial confidence in mapping pO_2 was estimated, using doses typical of fractionated radiotherapy.

2 Methods and Materials

2.1 Chemicals

PtG4 (platinum II G4) was provided by Sergei Vinogradov and colleagues.[23] MM2 was purchased from Luxcel Bioscience, Cork, Ireland,[25] bis(2-phenylbenzothiazolato)-(acetylaceto-nate)iridium(III) [Ir(btb)$_2$(acac)][26] was purchased from Sigma Aldrich, Saint Louis, Missouri, and Mito-ID intracellular oxygen sensor was purchased from Enzo Life Sciences, Farmingdale, New York. MDA-MB-231 luc-D3H2LN cells were obtained from Perkin Elmer (Waltham, Massachusetts) and PANC-1 cells were obtained from ATCC (CRL-1469, Manassas, Virginia). Dulbecco Modified Eagle Medium (DMEM), fetal bovine serum (FBS), phosphate buffered saline (PBS), and 0.05% trypsin were purchased from Thermo Fisher Scientific (Waltham, Massachusetts). Molecular Devices Gemini XS (Sunnyvale, California) was utilized for fluorescence plate reader measurements, Agilent Cary 50 UV-Vis (Santa Clara, California) was utilized for absorbance spectra, and Horiba Fluorolog-3 (Edison, New Jersey) was utilized for emission spectra. Fluorescence microscopy was performed on a Zeiss LSM 800 (Jena, Germany) confocal microscope.

2.2 Assessment of Absorbance and Fluorescence Emission Spectra

The absorbance and fluorescence emission spectra of PtG4 (1 μM, $\lambda_{ex} = 435$ nm, and $\lambda_{em} = 772$ nm), Ir(btb)$_2$(acac) (1 μM, $\lambda_{ex} = 337$, 480 nm, and $\lambda_{em} = 620$ nm), MM2 (1 μM, $\lambda_{ex} = 400$ nm, and $\lambda_{em} = 650$ nm), and MitoID (1 μM, $\lambda_{ex} = 380$ nm, and $\lambda_{em} = 650$ nm) were measured as validation prior to employing these reagents in cell and *in vivo* studies.

2.3 Cell Culture

PANC-1 cells and MDA-MB-231 luc-D3H2LN cells were grown in DMEM with 10% FBS in an incubator at 37°C with 5% CO_2, and 100% humidity and divided utilizing 0.05% trypsin when desired confluency was reached.

2.4 Fluorescence Assay In Vitro

PANC-1 cells were seeded in black 96-well plates with a clear bottom at 5000 cells/well. MM2, Ir(btb)$_2$(acac), and MitoID (10, 20, 30 μg/mL in PBS) were added to the cells and allowed to incubate for 24 h at 37°C. Media containing the reagents were removed and cells were rinsed with PBS. 10% FBS in PBS with or without glucose oxidase catalase oxygen scavenger (100 nM glucose oxidase, 1.5 μM catalase, and 56 mM glucose) was added after rinsing and the fluorescence intensity was analyzed with an excitation of 380 nm and emission of 660 nm. For limits of detection studies, 20, 2, 0.2, and 0.02 μg/mL of MM2 and Ir(btb)$_2$(acac) were utilized in the same fashion as described above. A student's t-test was utilized to assess differences in fluorescence between oxygenated versus oxygen scavenged conditions.

2.5 Cherenkov Imaging

Cherenkov emission was induced by a linear accelerator (Varian LINAC 2100CD, Palo Alto, California). The imaging system consisted of a time-gated intensified CCD camera (ICCD, PI-MAX4 1024i, Princeton Instruments) and a commercial lens (Canon EF 135 mm f/2L USM). The camera was focused on a mirror that reflected the imaging field $\sim$1 m away. The time-gated ICCD camera was synchronized to the radiation pulses ($\sim$3.25 μs duration and 360 Hz repetition rate) with the intensifier set as ×100 and turned on at a 4.26- or 1000-μs gate delay following each radiation pulse for phosphorescence or background measurement, and luminescence generated during 85.60-μs gate width (PtG4 and MM2), or 7.77 μs [Ir(btb)$_2$(acac)] was integrated via this ICCD. Images of the luminescence at different delay times between LINAC pulse and phosphorescence emission were acquired to construct emission lifetime. To maximize signal and minimize background interference, the room lights were shut off throughout these studies, and all lights in the room were masked off with black cloth and black tape.

2.6 CEL Studies In Vitro

Concentrations of 20, 2, 0.2, and 0.02 μg/mL of MM2, Ir(btb)$_2$(acac), MitoID, and PtG4 were utilized 96-well plate as above. For solution studies, 300 μL of each solution with and without oxygen scavenger were utilized. For cellular studies, PANC-1 cells were seeded in black 96-well plates with a clear bottom at 5000 cells/well. The reagents were added to the cells and allowed to incubate for 24 h at 37°C. Media containing the reagents were removed and cells were rinsed with PBS. 10% FBS in PBS was added after rinsing.

2.7 General Animal Imaging

All animal procedures were approved by the Institutional Animal Care and Use Committee, and the studies here were carried out in compliance with these approved procedures.

2.8 In Vivo Imaging

Briefly, 10^5 MDA-MB-231 luc-D3H2LN cells were injected under the skin on the flank of a nude mouse (two tumors per mouse, eight tumors per reagent studied). After $\sim$3 weeks of growth, animals were chosen for use when their tumor was $\sim$6 × 6 × 3 mm^3 in size. The CELSI scan was completed vertically. Images of the luminescence at different delay times between LINAC pulse and phosphorescence emission were acquired to construct emission lifetime. Under general anesthesia of inhaled isofluorane, 50 μL of 50 μM of each reagent was directly injected into the tumors and the animal was imaged alive and then again at 30 min after euthanize, which allows determination of emission lifetime at ambient pO_2 (alive) low pO_2 environments (dead), respectively.

2.9 Statistical Analysis

The tissue pO_2 was determined utilizing the Stern–Volmer relationship. The differences between the live and dead conditions, as shown in Fig. 5 with $n = 8$ paired samples each, were assessed using a two-tailed Students t-test, with $\alpha = 0.05$ and resulting $P < 0.001$. This shows that there are significant differences between the values of both emission lifetime and
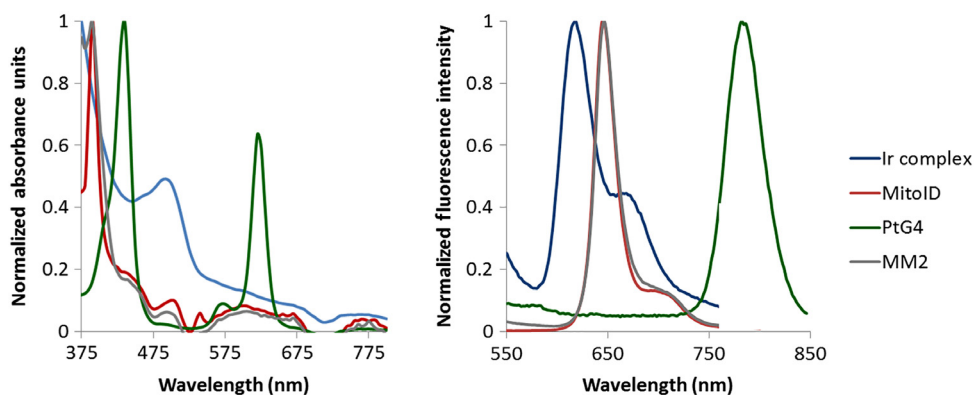
Fig. 1 Absorbance and emission spectra for oxygen sensors. The absorbance and fluorescence emission spectra for Ir(btb)$_2$(acac) (blue), MitoID (red), PtG4 (green), and MM2 (gray).
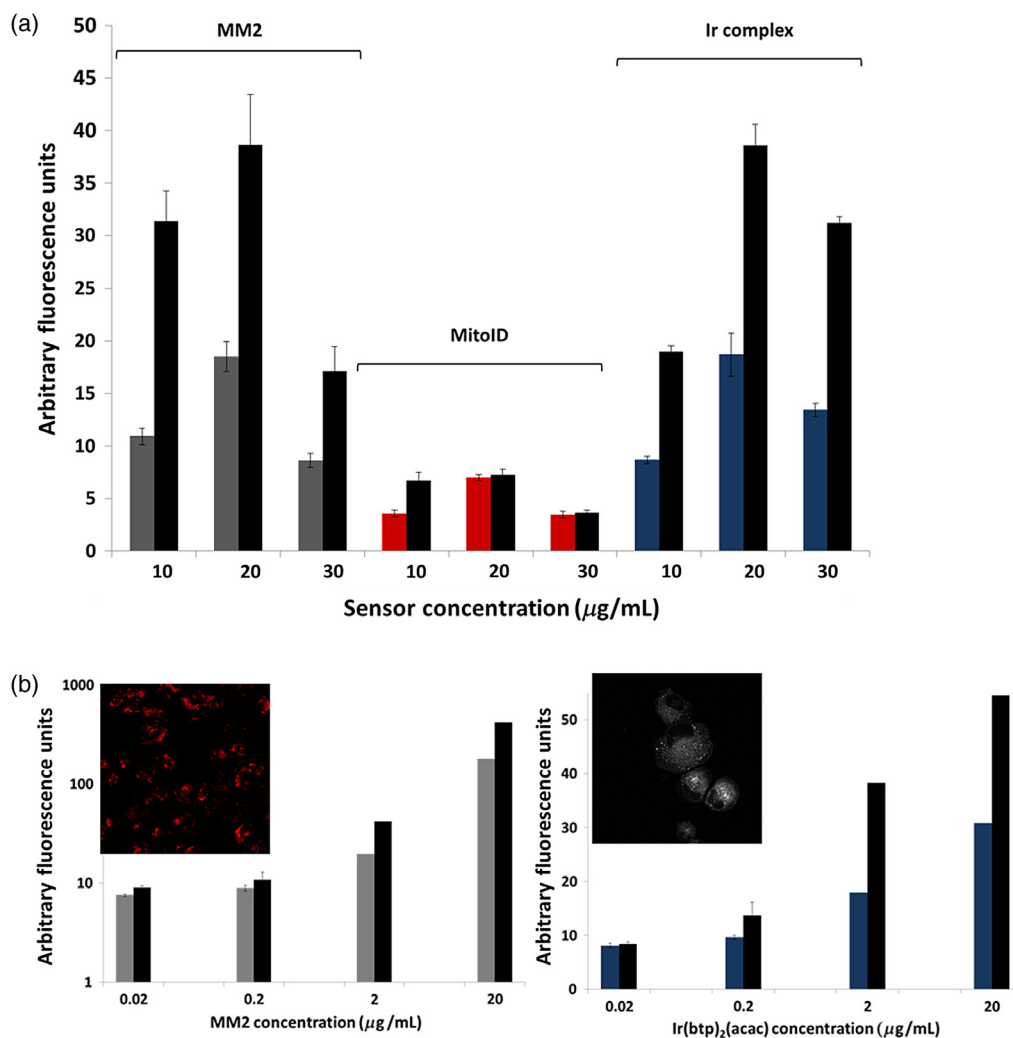

Fig. 2 Comparison of commercially available oxygen sensors in PANC-1 cells. (a) MM2 (gray), MitoID (red), and Ir(btb)$_2$(acac) (blue) were incubated with PANC-1 cells overnight. Fluorescence was measured in the presence of ambient oxygen [light gray, MM2, medium gray, MitoID, and dark gray, Ir(btb)$_2$(acac)] and with glucose oxidase catalase enzymatic oxygen scavenging (black). (b) The brightest commercial oxygen sensors were explored at decreasing concentrations (20, 2, 0.2, and 0.02 μg/mL) to determine the lowest concentration that can be detected. Inset shows fluorescence microscopy of each sensor (20 μg/mL) loaded into PANC-1 cells. Excitation and emission were measured at 380 and 660 nm, respectively. The fluorescence intensity represents the average of six experiments $\pm$SEM.

pO_2 of the animals alive versus dead. Figure 5 was generated using Python 3.4.3 with the library matplotlib 2.0.0.

3 Results

The set of four phosphorescent oxygen sensors were directly compared to determine which of these reagents would be ideal for use in CELSI in tumors. These agents were chosen based upon published data, and they represented the most promising mix of agents for use *in vivo* with longer lifetime emission from phosphorescence. The absorbance and emission spectra of PtG4 (green), MM2 (gray), $Ir(btb)_2(acac)$ (blue), and MitoID (red) are shown in Fig. 1.[25,26] Relative brightness of the commercially available MM2, $Ir(btb)_2(acac)$, and MitoID was assessed at increasing concentrations (10, 20, and 30 μg/mL) in PANC-1 cells in the presence and absence of ambient oxygen, through the addition of the enzymatic oxygen-scavenging system of glucose oxidase and catalase (GODCAT). Measurements of emission were taken via fluorescence plate reader. MM2 and $Ir(btb)_2(acac)$ exhibited the maximum signal under deoxygenated conditions at 20 μg/mL, and the MitoID intensity in the presence and absence of oxygen scavengers was lower in comparison [Fig. 2(a)]. Statistically significant changes in oxygenation can be detected at concentrations as low as 0.2 μg/mL for $Ir(btb)_2(acac)$ and 0.02 μg/mL for MM2 [Fig. 2(b)], as assessed by a student's t-test.

We sought to evaluate the effectiveness of these reagents to be imaged with Cherenkov excited luminescence (CEL). Solutions of PtG4, MM2, $Ir(btb)_2(acac)$, and MitoID at decreasing concentrations (20, 2, 0.2, and 0.02 μg/mL) were placed in a 96-well plate with and without GODCAT and evaluated via epiluminescence. The background corrected phosphorescence intensities from this experiment at the maximum concentration of 20 μg/mL are as follows (first number for each compound represents ambient oxygen, second number represents GODCAT): MM2 (565, 1349); PtG4 (230, 1269); $Ir(btb)_2(acac)$ (45.7, 168); MitoID (119, 150) [Fig. 3(a)]. This experiment was repeated by loading all of these reagents into PANC-1 cells with and without GODCAT and imaging via CEL. The phosphorescence intensities from this experiment at the maximum concentration of 20 μg/mL are as follows (first number for each compound represents the signal under ambient

oxygen, and the second number is the signal deoxygenated with GODCAT): MM2 (153, 376); PtG4 (181, 406); $Ir(btb)_2(acac)$ (235, 633); MitoID (223, 288) [Fig. 3(b)].

A murine experiment to sense tissue oxygenation was completed in mice with subcutaneous MDA-MB-231luc-D3H2LNtumors. The setup for CELSI is shown in Figs. 4(a) and 4(b). Briefly, gantry head of the linear accelerator that delivers the radiation is positioned below the mouse, which is located on the treatment couch. A mirror is placed that redirects the photons to the ICCD camera for imaging. A total of four tumors per compound were imaged, with local injection of 50 μL of each reagent [50 μM PtG4, 2.5 nmol, 1.75 mg per tumor and 50 μM $Ir(btb)_2(acac)$, 2.5 nmol, 35 μg per tumor]. Each mouse was imaged while alive and then repeated 30 min after euthanasia to capture both normoxic and hypoxic conditions, respectively. In the euthanized animal, the drop in blood circulation and respiration causes a dramatic decrease in pO_2 values. Temperature was controlled using a heating pad under each animal, throughout the study, and the CELSI scan was completed vertically for these cases. Images of the luminescence were captured at different delay times after the LINAC pulse to determine emission lifetimes for each reagent. The maximum intensity projection images of CELSI from both PtG4 and $Ir(btb)_2(acac)$ at a delay time of 4.26 μs are shown in Fig. 4(c). A comparison of the intensity differences between PtG4 phosphorescence at various delay times in an alive and dead mouse are shown in Fig. 5(a). The emission lifetimes were mapped for the alive and euthanized mouse for PtG4 and are quantified and displayed via a box and whiskers plot [Fig. 5(b)]. Using the Stern–Volmer equation, we estimated the average tissue pO_2 with the reported quenching constant for PtG4[27] [Fig. 5(c)]. The phosphorescence at different delay times for a euthanized mouse is shown for $Ir(btb)_2(acac)$ [Fig. 5(d)]. In addition, we created a map of emission lifetimes and estimated the average pO_2 using the reported quenching constant for $Ir(btb)_2(acac)$ using the Stern–Volmer relationship.[14]

4 Discussion

Due to the redshifted emission of PtG4 (772 nm) in comparison to the other reagents, it was originally hypothesized that this reagent would be the most effective for imaging in tumors
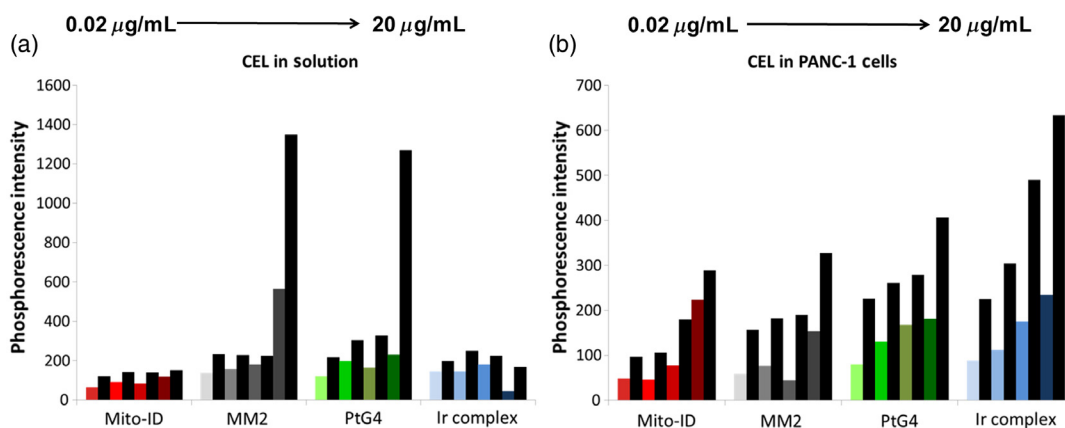

Fig. 3 Comparison of CEL with phosphorescent oxygen sensors. Increasing concentrations of each sensor indicated by darker shades of each color [0.02, 0.2, 2, and 20 μg/mL, MitoID (red), MM2 (gray), PtG4 (green), and $Ir(btb)_2(acac)$ (blue)] were analyzed in ambient oxygen or with enzymatic oxygen scavenger glucose oxidase/catalase (black). A 96-well plate with these reagents in (a) solution or (b) loaded into PANC-1 cells was exposed to 6-MV radiation from a LINAC, and the phosphorescence intensity was measured via ICCD.
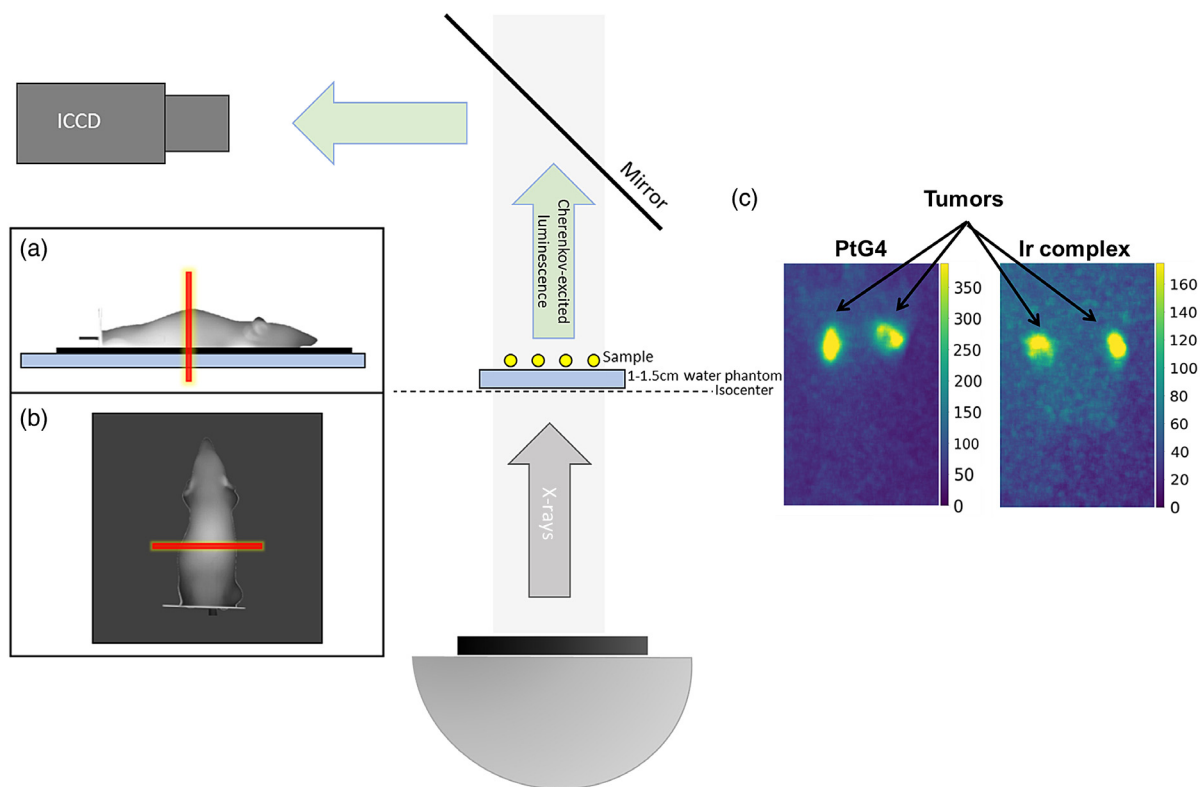
Fig. 4 CELSI setup and *in vivo* imaging with PtG4 and Ir(btb)$_2$(acac). The LINAC gantry head that delivers radiation is placed below the mouse that is positioned on the treatment couch. A mirror above redirects the photons to the ICCD. (a) Lateral view of the mouse depicting passage of radiation sheet in red (b) aerial view as imaged from the ICCD camera. (c) Under anesthesia of isofluorane, 2.5 nmol of each reagent was injected into subcutaneous MDA-MB-231luc-D3H2LN tumors. Maximum intensity projection of PtG4 and of Ir(btb)$_2$(acac) at 4.26 μs delay time, respectively. Tumors are indicated with line arrows.

since this wavelength would achieve the most effective tissue penetration. However, we wanted to compare PtG4 with other commercially available phosphorescent oxygen sensors to identify the reagents with the best qualities for utilization in CELSI. Several factors are involved in the selection of ideal compounds. As with fluorescence imaging, the quantum yield of the compound is a significant factor that determines the efficiency of imaging. In CEL imaging, time gating is used to separate Cherenkov emissions from luminescence, so luminescence lifetime is also important to consider. Medical LINACs have a 4-μs radiation pulse, and so this moderate pulse time limits the time gating to the microsecond regime, and without significant change to the LINAC or acquisition, nanosecond lifetimes would not be possible to measure. The luminescent agents that are available with microsecond lifetimes are typically phosphorescent. It has not been feasible to detect fluorescent agents that have nanosecond lifetimes, other than through wavelength filtering and continuous wave detection.[21] The typical timing used for image acquisition that is coupled to the LINAC is shown in Fig. 6(a). Experimentally, the gate width is generally set between 5 and 10 times the deoxygenated lifetime of the reagent of interest (τ_0). The CEL is then detected at multiple delay times in order to determine the emission lifetime of each phosphorescent agent. The time between radiation pulses is one factor that will limit the maximum lifetime when choosing a phosphorescent compound. The LINAC generates radiation pulses at a repetition rate between 2.7 and 17 ms (600 to 100 MU/min). Shorter lifetimes can be difficult

to discriminate from the radiation-induced Cherenkov light. The LINAC radiation pulse does not immediately turn off, and both stray charge and Cherenkov emissions may be detected during the transition phase. Phosphorescent compounds with lifetimes in this range (<4.5 μs) will be difficult to detect. A plot of the decay curves depicting lifetime measurements as a function of quantum yield for each compound used in the study is shown in Fig. 6(b). Ir(btb)$_2$(acac) has been utilized in LED applications and has a high quantum yield of 0.33,[26] which should also impart ideal imaging properties; however, its shorter emission lifetime of 5.8 μs[26] may limit its application in CELSI. While PtG4, MM2, and MitoID have lower quantum yields, their longer emission lifetimes should be advantageous for signal detection. In addition, MM2 and MitoID are nanoparticles with multiple copies of oxygen-sensitive porphyrins,[25] which should provide enhanced signal-to-noise ratio.

With optimization in mind, a comparison of commercially available oxygen sensors was completed *in vitro*, comparing signals in ambient oxygen to that in the presence of oxygen-scavenging GODCAT. These conditions were employed since phosphorescent oxygen sensors exhibit maximum luminescence in the absence of oxygen. PtG4 was not employed in this study since the maximum cutoff for the fluorescence emission of the plate reader is shorter than the PtG4 fluorescence emission. As expected, these reagents show a signal enhancement in the presence of GODCAT conditions, indicating a response to change in oxygenation levels. MM2 and Ir(btb)$_2$(acac) gave the most robust responses in sensing oxygen changes via steady state
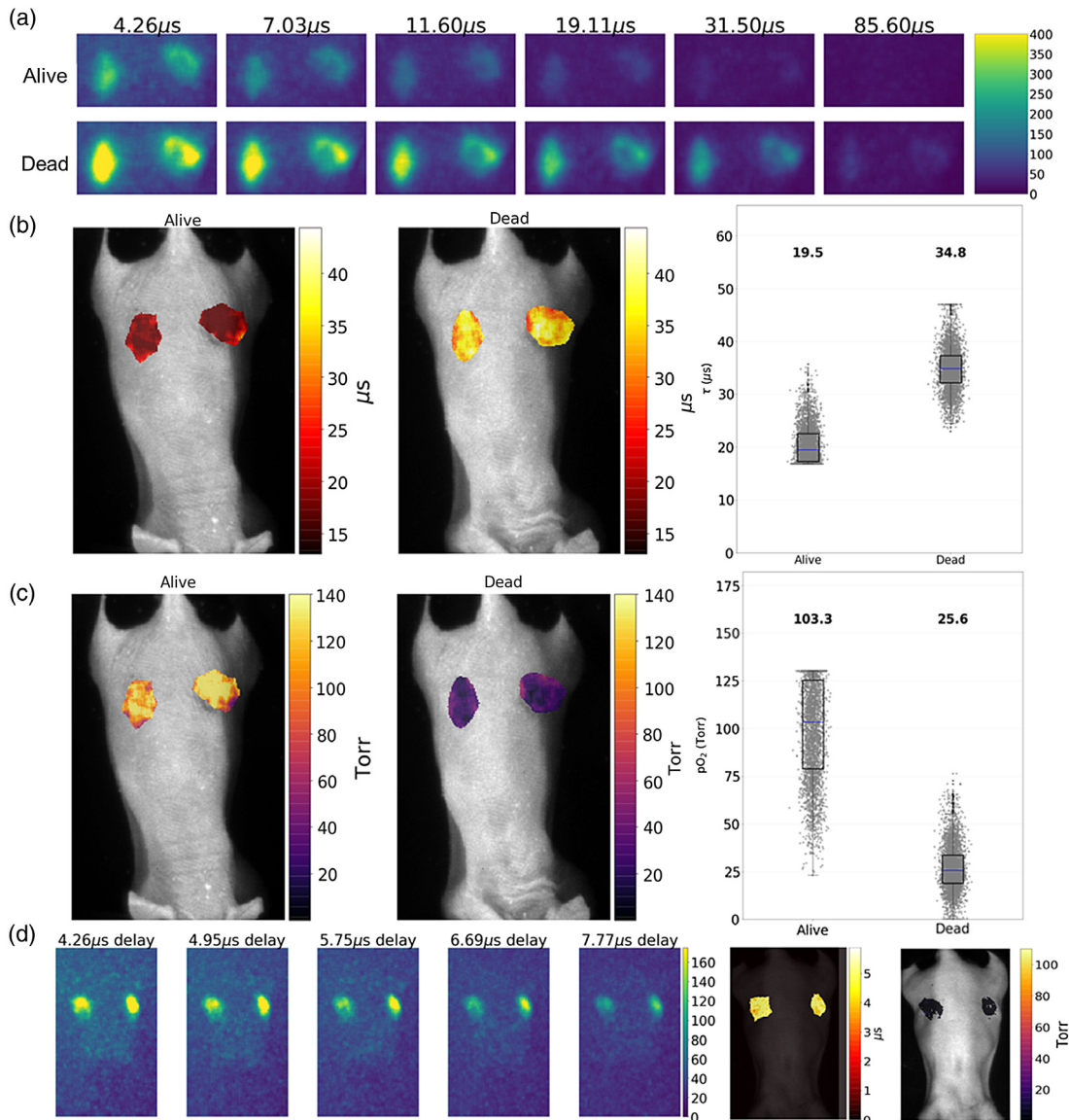
Fig. 5 *In vivo* lifetime imaging with PtG4 and $Ir(btb)_2(acac)$. Under anesthesia of isofluorane, the animal was imaged at various delay times based on reported lifetimes of each reagent to gain emission lifetime information alive and 30 min after euthanize, when the drop in blood circulation and respiration causes a marked decrease in pO_2 values. (a) Comparison of PtG4 phosphorescence intensity at various delay times based on known PtG4 emission lifetime in subcutaneous tumors alive (top) and 30 min after euthanize(bottom). (b) PtG4 emission lifetime maps and box and whiskers plot of emission lifetimes of alive and euthanized mouse. (c) pO_2 maps and box and whiskers plot of oxygen levels in alive and euthanized mouse for PtG4. (d) Phosphorescence intensity of tumors injected with $Ir(btb)_2(acac)$ at different delay times informed from the reported $Ir(btb)_2(acac)$ emission lifetime, map of emission lifetime, and pO_2 map in euthanized mouse. All lifetime maps and subsequent pO_2 maps for both reagents were constructed utilizing data from the 4.26-μs delay time.

fluorescence [Fig. 2(a)]. At the highest concentration utilized (30 μg/mL), the signal was attenuated in comparison to the 20 μg/mL samples, which could be attributed to self-quenching, although further investigation of this was not done. Due to these observations, since MM2 and $Ir(btb)_2(acac)$ gave the best signal, the next focus was to determine the lowest concentration of each sensor that could be utilized to detect oxygen levels *in vitro*. We found that $Ir(btb)_2(acac)$ still elicited a luminescence signal in response to oxygen changes in PANC-1 cells at 0.2 μg/mL. While MM2 exhibited a statistically significant response to oxygen scavenging conditions at a lower

concentration (0.02 μg/mL), the responses to oxygenation changes were not robust at concentrations lower than 2 μg/mL [Fig. 2(b)].

We investigated CEL both in solution and loaded into PANC-1 cells of the previously studied PtG4 as well as MM2, $Ir(btb)_2(acac)$, and MitoID. Both PtG4 and MM2 exhibited strong phosphorescence at 20 μg/mL in solution, particularly with oxygen scavenging, when excited by Cherenkov emission, with phosphorescence intensities of 1349 and 1269, respectively, whereas $Ir(btb)_2(acac)$ and MitoID did not display significant phosphorescence in solution, with intensities of 250 and
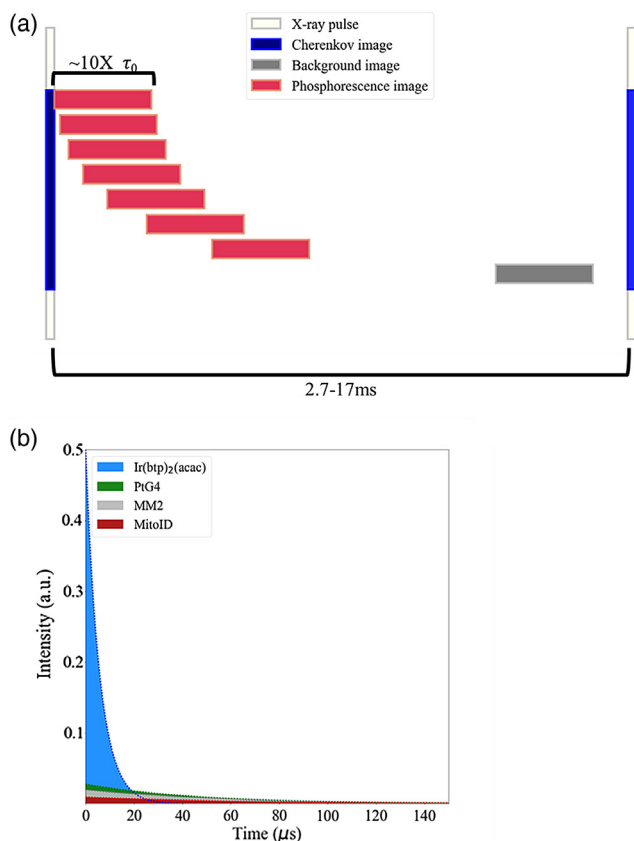
Table 1 Side-by-side comparison of phosphorescent oxygen sensors utilized for CEL.

Compound	CEL solution	CEL cells	CELSI in vivo	Biomolecule interaction	Stability	Self-quenching
PtG4	+	+	+	−	+	−
Ir(btb)$_2$(acac)	+	+	+	+	+	+
MM2	+	+	−	−	−	+
MitoID	−	+	−	+	−	+

Fig. 6 Considerations for CELSI. (a) Cherenkov imaging timing. Experimentally, the gate width is generally set between 5 and 10 times the deoxygenated lifetime (τ_0) of the reagent of interest. Luminescence is detected at a series of delay times (red blocks) after the Cherenkov emission (blue column) to assess the emission lifetime of phosphorescent agents. The LINAC generates radiation pulses at a repetition rate between 2.7 and 17 ms (600 to 100 MU/min). (b) Plot of emission decay curves as a function of quantum yield.

150, respectively [Fig. 3(a)]. We have previously seen excellent results with CELSI with PtG4,[19,21,22] and since MM2 contains multiple copies of a porphyrin grafted to a nanoparticle, enhanced signal in response to oxygen was anticipated for both of these reagents. As expected, we found that the intracellular phosphorescence intensity was markedly decreased in comparison to the phosphorescence measured in solution. Interestingly, Ir(btb)$_2$(acac) exhibits a much better phosphorescence signal in cells versus solution, giving the largest detectable signal in comparison to the other reagents [Fig. 3(b)]. This is likely due to the fact that this complex binds to albumin or another cellular protein, thereby enhancing permeability. However, previous reports indicate that it is no longer sensitive to oxygen when bound to albumin *in vitro*. Our results and other cell studies with Ir(btb)$_2$(acac) that show oxygen sensitivity indicate that binding to albumin is not the mechanism that imparts enhanced signal in cells versus solution.[26] The performance of MM2 was diminished intracellularly, possibly due to lower cell permeability than Ir(btb)$_2$(acac). In fact, Ir(btb)$_2$(acac) was found to penetrate cells far more rapidly than MM2 (30 min versus 24 h). PtG4 gave a robust response to oxygenation changes in cells; however, the intensity was somewhat attenuated in comparison to Ir(btb)$_2$(acac). One critical advantage of PtG4 is that the dendrimer shell prevents its

interaction with other biomolecules that could potentially perturb its emission lifetime and thus pO$_2$ estimations. This is considered to be a key factor in making this agent a linear reporter of tissue pO$_2$, and in fact PtG4 and similar reagents have been calibrated appropriately in extensive studies.[19–24,27] While MitoID displays an enhanced signal in cells versus solution, it still elicits the weakest phosphorescent response to changes in oxygen concentration.

PtG4, Ir(btb)$_2$(acac), and MM2 seemed to have promise for use in CELSI. Therefore, we investigated these reagents for sensing oxygenation levels in subcutaneous tumors. We were unable to detect significant phosphorescence with MM2 *in vivo*. However, we were able to sense emission lifetime and as such calculate tissue oxygenation utilizing CELSI for both PtG4 and Ir(btb)$_2$(acac) at the nmol level [Figs. 5(b)–5(d)]. Unfortunately, we were not able to measure fluorescence lifetime or tissue pO$_2$ in live mice with Ir(btb)$_2$(acac). This is likely because the luminescence lifetime in a fully oxygenated sample of Ir(btb)$_2$(acac) is shorter than we can detect since the shortest delay time feasible for imaging after the radiation pulse is 4.26 μs. We also observed quenching with Ir(btb)$_2$(acac) at concentrations higher than 50 μM in subcutaneous tumors, as we did in the fluorescence plate reader experiments.

A summary of the results as well as a comparison of the pros and cons of the oxygen sensors we utilized for this study are provided in Table 1. Briefly, both PtG4 and Ir(btb)$_2$(acac) are stable indefinitely, whereas MM2 and MitoID nanoparticles have a short shelf life of only 1 to 2 weeks once resuspended. PtG4 has a dendrimer shell that prevents its interaction with biomolecules, allowing accurate determinations of fluorescence lifetime and pO$_2$ calculations. Ir(btb)$_2$(acac) and MitoID appear to interact with biomolecules in some way, given the difference in phosphorescent intensities discovered in solution versus cells. Finally, we have observed that MM2, MitoID, and Ir(btb)$_2$(acac) exhibit self-quenching at higher concentrations, where we have not seen this effect with increasing concentrations of PtG4.

5 Conclusion

When used *in vitro* in PANC-1 cells at the same concentrations, the signal strengths suggest that the optimal agents would be Ir(btb)$_2$(acac), followed by PtG4, and then MM2 and MitoID. However, *in vivo*, only PtG4 and Ir(btb)$_2$(acac) were found to be measurable at nmol doses in the tumors, and assessment of tissue oxygenation accomplished. On the timescale of LINAC produced x-ray imaging, PtG4 is the more ideal agent because of the lifetime on the scale of tens of microseconds versus Ir(btb)$_2$(acac), which has a lifetime

of a few microseconds, which hinders detection at higher tissue pO_2 values. This work represents: (1) a unique way to harness Cherenkov emission for imaging purposes in conjunction with radiotherapy, (2) a noninvasive determination of tumor pO_2, and (3) a direct comparison of phosphorescent sensors available to probe tissue oxygenation.

Disclosures

The authors report no conflicts of interest.

Acknowledgments

References

1. P. Vaupel, A. Mayer, and M. Hockel, "Impact of hemoglobin levels on tumor oxygenation: the higher, the better?" *Strahlenther. Onkol.* **182**(2), 63–71 (2006).

2. S. M. Evans and C. J. Koch, "Prognostic significance of tumor oxygenation in humans," *Cancer Lett.* **195**(1), 1–16 (2003).

3. J. Bussink et al., "Effects of nicotinamide and carbogen on oxygenation in human tumor xenografts measured with luminescense based fiber-optic probes," *Radiother. Oncol.* **57**(1), 21–30 (2000).

4. A. Turaka et al., "Hypoxic prostate/muscle ratio predicts for outcome in patients with localized prostate cancer: long-term results," *Int. J. Radiat. Oncol. Biol. Phys.* **82**(3), e433–e439 (2012).

5. P. Vaupel and D. K. Kelleher, "Blood flow and oxygenation status of prostate cancers," *Adv. Exp. Med. Biol.* **765**, 299–305 (2013).

6. O. Genbacev et al., "Human cytotrophoblast expression of the von Hippel–Lindau protein is downregulated during uterine invasion in situ and upregulated by hypoxia in vitro," *Dev. Biol.* **233**(2), 526–536 (2001).

7. C. J. Koch, "A two-component assay for hypoxia incorporating long-term nitroreduction and short-term DNA-damage allows differentiation of the three hypoxia sub-types," *Radiat. Res.* **190**(1), 72–87 (2018).

8. S. K. Loftus et al., "Hypoxia-induced HIF1α targets in melanocytes reveal a molecular profile associated with poor melanoma prognosis," *Pigm. Cell Melanoma Res.* **30**(3), 339–352 (2017).

9. H. B. Stone and H. R. Withers, "Tumor and normal tissue response to metronidazole and irradiation in mice," *Radiology* **113**(2), 441–444 (1974).

10. K. Y. Aguilera and R. A. Brekken, "Hypoxia studies with pimonidazole in vivo," *Bio-Protocol* **4**(19), e1254 (2014).

11. M. R. Gonçalves et al., "Decomposition of spontaneous fluctuations in tumour oxygenation using BOLD MRI and independent component analysis," *Br. J. Cancer* **113**(8), 1168–1177 (2015).

12. D. Li et al., "Correlation between BOLD-MRI and HIF expression level in renal carcinoma," *Int. J. Clin. Exp. Pathol.* **8**(10), 13759–13763 (2015).

13. H. Gustafsson et al., "EPR oximetry of cetuximab-treated head-and-neck tumours in a mouse model," *Cell Biochem. Biophys.* **75**(3–4), 299–309 (2017).

14. H. M. Swartz, The measurement of oxygen in vivo using EPR techniques, in *In Vivo EPR (ESR): Theory and Application*, L. J. Berliner, Ed., pp. 403–440, Springer US, Boston, Massachusetts (2003).

15. S. Srinivasan et al., "In vivo hemoglobin and water concentrations, oxygen saturation, and scattering estimates from near-infrared breast tomography using spectral reconstruction," *Acad. Radiol.* **13**(2), 195–202 (2006).

16. O. J. Kelada et al., "Quantification of tumor hypoxic fractions using positron emission tomography with [(18)F]fluoromisonidazole ([(18)F]FMISO) kinetic analysis and invasive oxygen measurements," *Mol. Imaging Biol.* **19**(6), 893–902 (2017).

17. S. Stieb et al., "Longitudinal PET imaging of tumor hypoxia during the course of radiotherapy," *Eur. J. Nucl. Med. Mol. Imaging* **45**(12), 2201–2217 (2018).

18. A. K. Glaser et al., "Projection imaging of photon beams by the Cerenkov effect," *Med. Phys.* **40**(1), 12101 (2013).

19. R. Zhang et al., "Cerenkov radiation emission and excited luminescence (CREL) sensitivity during external beam radiation therapy: Monte Carlo and tissue oxygenation phantom studies," *Biomed. Opt. Express* **3**(10), 2381–2394 (2012).

20. R. Zhang et al., "Superficial dosimetry imaging based on Cerenkov emission for external beam radiotherapy with megavoltage x-ray beam," *Med. Phys.* **40**(10), 101914 (2013).

21. H. Lin et al., "Comparison of Cherenkov excited fluorescence and phosphorescence molecular sensing from tissue with external beam irradiation," *Phys. Med. Biol.* **61**(10), 3955–3968 (2016).

22. R. Zhang et al., "Oxygen tomography by Cerenkov-excited phosphorescence during external beam irradiation," *J. Biomed. Opt.* **18**(5), 50503 (2013).

23. T. V. Esipova et al., "Two new 'protected' oxyphors for biological oximetry: properties and application in tumor imaging," *Anal. Chem.* **83**(22), 8756–8765 (2011).

24. R. I. Dmitriev and D. B. Papkovsky, "Intracellular probes for imaging oxygen concentration: how good are they?" *Methods Appl. Fluoresc.* **3**(3), 34001 (2015).

25. R. I. Dmitriev and D. B. Papkovsky, "Optical probes and techniques for O_2 measurement in live cells and tissue," *Cell Mol. Life Sci.* **69**(12), 2025–2039 (2012).

26. S. Zhang et al., "Phosphorescent light-emitting iridium complexes serve as a hypoxia-sensing probe for tumor imaging in living animals," *Cancer Res.* **70**(11), 4490–4498 (2010).

27. C. T. Sullender et al., "Imaging of cortical oxygen tension and blood flow following targeted photothrombotic stroke," *Neurophotonics* **5**(3), 035003 (2018).

Biographies of the authors are not available.